applied sciences

MDPI

Article

Enhancing Hydrophobicity of Nanocellulose-Based Films by Coating with Natural Wax from *Halimium viscosum*

Ana Ramos [1,*], Jesus M. Rodilla [1], Rodrigo Ferreira [1] and Ângelo Luís [2,*]

[1] Department of Chemistry and Fiber Materials and Environmental Technologies Research Unit (FibEnTech), University of Beira Interior, Rua Marquês d'Ávila e Bolama, 6201-001 Covilhã, Portugal; rodilla@ubi.pt (J.M.R.); rodrigo.ferreira@ubi.pt (R.F.)

[2] RISE-Health, Department of Medical Sciences, Faculty of Health Sciences, University of Beira Interior, Av. Infante D. Henrique, 6200-506 Covilhã, Portugal

* Correspondence: ammr@ubi.pt (A.R.); angelo.luis@fcsaude.ubi.pt (Â.L.)

Abstract

This study aimed to improve the hydrophobicity of cellulose nanofibril (CNF) films using a natural wax coating. For this purpose, firstly, the selection, extraction and characterization of a natural wax and fatty acids were carried out. These compounds were extracted from the aerial part of the *Halimium viscosum* plant. The chromatogram resulting from the chemical analysis of the extract revealed the presence of 15 compounds, with nonacosane being the major compound present. For film production, two different chemical pulps gels (sulfite and sulfate) were first characterized in terms of solids content, rheology and Fourier transform infrared spectroscopy (FTIR). The CNF films were produced by the solvent casting method, coated on one side with the extracted wax and subsequently characterized by wettability, surface energy, differential scanning calorimetry (DSC), FTIR, structural properties and water vapor permeability. The results showed that the wax-coated films exhibited a significant increase in water resistance, with a water contact angle exceeding 100°, demonstrating improved hydrophobicity. Also, the water vapor transmission rate (WVTR) of the films was drastically reduced after wax coating. Furthermore, the coated films maintained good transparency, making them a viable alternative to synthetic plastic. This study highlights the potential of natural wax coatings to improve the moisture barrier properties of biodegradable CNF films, promoting their application in sustainable packaging solutions.

Keywords: cellulose nanofibrils; natural wax; hydrophobicity; biodegradable films; coating

Academic Editors: Wenluan Zhang and Yumin Huang

Received: 4 June 2025
Revised: 1 July 2025
Accepted: 4 July 2025
Published: 6 July 2025

Citation: Ramos, A.; Rodilla, J.M.; Ferreira, R.; Luís, Â. Enhancing Hydrophobicity of Nanocellulose-Based Films by Coating with Natural Wax from *Halimium viscosum*. *Appl. Sci.* **2025**, *15*, 7576. https://doi.org/10.3390/app15137576

1. Introduction

Since the publication of the first scientific work on nanocellulose-based films [1], cellulose nanofibrils (CNFs) have attracted the attention of researchers worldwide. Nanocellulose possesses excellent physicochemical properties and is derived from the most abundant natural polymer on Earth. Moreover, it is both renewable and biodegradable, making it an environmentally friendly material [2].

Nanocellulose can be obtained from various sources rich in cellulose, such as wood pulps (sulfate or sulfite), agricultural residues and marine biomass. Usually, production involves a chemical pre-treatment step, such as acid hydrolysis, oxidation or enzymatic treatment, followed by an intensive mechanical process, such as homogenization, grinding or ultrasonication, which promotes the fibrillation of cellulose fibers. Nanocellulose can

be obtained in distinct forms, such as gel or colloidal suspension, depending on the concentration and degree of dispersion of the fibrils [3].

In the present work, the nanocelluloses were obtained from bleached eucalyptus pulp, produced by two distinct chemical processes, sulfite and sulfate. The sulfate process uses an alkaline solution of sodium hydroxide (NaOH) and sodium sulfide (Na_2S). The sulfite process involves an acidic solution containing bisulfite (HSO_3^-) and magnesium cation (Mg^{2+}). Subsequently, both pulps were subjected to an oxidative TEMPO process, followed by identical mechanical treatment in the homogenizer.

From the nanocellulose gels, it is possible to produce films with high transparency and high mechanical resistance [4,5]. Despite these excellent attributes, required in a wide range of applications such as sustainable packaging, electronic devices, medicinal applications, membranes, among others, the performance of CNF-based films is still inferior to synthetic plastic concerning water sensitivity. Knowledge gaps still exist, especially for food packaging applications [6].

This weakness seriously limits the practical use of this biopolymer in a wide range of food packaging. However, these films can provide an alternative to plastic regarding biodegradability and waste reduction [7].

Nanocellulose itself has a hydrophilic nature due to the presence of hydroxyl groups (–OH) on its surface presenting limitations in applications that require resistance to humidity. This drawback can be changed using chemical/physical modifications of nanocelluloses [8]. Research in this area continues to foster the development of eco-friendly materials that meet industry requirements [7]. Hydrophobization techniques, such as the application of a hydrophobic layer of calcium carbonate modified with stearic acid on CNF films, has shown promising improvements in creating effective moisture resistance [9]. The layer-by-layer (LbL) technique allows the application of ultra-thin coats of hydrophobic polymers, like waxes, promoting effective water resistance [10]. In this work, a LbL assembly using natural components, including carnauba wax particles, demonstrated to produce hydrophobic coatings on CNF films. These methods allow for moisture barriers without significantly increasing thickness. Also, it was previously demonstrated that wax coatings could be a way to increase the moisture resistance of nanocellulose films and improve their hydrophobicity [11]. A strategy that seems to overcome one of the greatest weaknesses of CNF films, its hydrophilicity, seems to be the combination of nanocellulose with hydrophobic products such as natural waxes. Natural waxes are lipids, whose chemical composition presents a mixture of hydrocarbons, free fatty acids, fatty alcohols, esters, ketones and sterols. A good understanding of the chemical composition is of the highest importance since wax can vary depending on its origin and extraction methods [12]. The use of bio-based waxes and synthetic hydrophobic polymers is important in this context, as they achieve hydrophobicity without sacrificing biodegradability. Nevertheless, one of the current challenges concerns the balance between hydrophobicity and other important properties, namely the transparency of films, as increased hydrophobicity can sometimes reduce clarity.

In this study, the effect of a natural wax coating (WC) on CNF films regarding their hydrophobization was investigated. Firstly, wax was extracted and characterized and then applied to one side of CNF films. The films were previously prepared using two nanocellulose gels, CNF1 and CNF2, respectively, from sulfite and sulfate pulps. Coated and uncoated films were then characterized.

2. Materials and Methods

2.1. Wax Extraction

The waxes were obtained from the leaves and aerial part of the *Halimium viscosum* plant, collected in Celorico da Beira, Portugal. After a drying process at room temperature, the aerial part was extracted with hot hexane (Merck, Darmstadt, Germany) in Soxhlet. The hexane extract obtained was dissolved in hot methanol and, upon slow cooling, the plant waxes, made up of a mixture of compounds, were precipitated and then used for application in films.

2.2. Hydrolysis of Waxes

In 100 mL round bottom flasks, 20 g of wax sample were placed to hydrolyze, 50 mL of methanol were added and then a solution of 3.0 g of sodium hydroxide was dissolved in 20 mL of methanol (Merck, Darmstadt, Germany). This mixture was allowed to stir for 24 h. After that, the methanol present in the flasks was removed using a rotary evaporator (Büchi, Barcelona, Spain) and then placed in a decantation funnel, where dichloromethane (Merck, Darmstadt, Germany) was added to ensure phase separation. The dichloromethane was decanted, and the extraction process was repeated until there was no more interphase. The organic part was separated, where the products that were not hydrolyzed were present, and the neutral products (Neutral Part) were dried over anhydrous sodium sulfate (Merck, Darmstadt, Germany) and then the solvent was evaporated. These neutral part products can also be used for application in films.

2.3. Extraction of Fatty Acids

Then 2 M HCl (Merck, Darmstadt, Germany) was added to the aqueous solution from the previous extraction of neutral products until a solution with pH = 2 was obtained. Then this aqueous part was extracted 3 times with dichloromethane, to remove the free fatty acids (Acidic Part).

2.4. Characterization of Waxes

To identify the main components of the wax, a chemical analysis was performed on an Agilent 7890A GC chromatograph associated with an XLMSD MS A 5975C inert mass spectrometer (Santa Clara, CA, USA). The ionization technique used was a 70 eV electron impact. The column used was a J & W DB5-ms, 30 m long, 0.25 mm in diameter and 0.25 μm film thick, programmed to reach a temperature of 60 °C in 5 min and reach 250 °C, with a flow rate of 10 °C per min. The injector temperature was 250 °C, the source temperature was 230 °C, the interface temperature was 280 °C, the quadrupole temperature was 180 °C and the flow rate was 1 mL/min, using helium as the carrier gas.

2.5. Characterization of Nanocellulose Gels

As starting materials, two nanocellulose gels (CNF_1 and CNF_2) were used. Both gels were obtained from bleached chemical pulps of eucalyptus globulus; the first came from a sulfite pulp and the second from a sulfate pulp. Both pulps were subjected to a similar TEMPO (2,2,6,6,-tetramethylpiperidine-1-oxyl) oxidative process, with a hydromodulus of 1:100. For sulfite pulp, the following system was used: 0.016 g TEMPO/0.1 g NaBr/33.3 mL NaClO (Merck, Darmstadt, Germany). NaClO was added in four spaced additions of 1 h at room temperature and pH higher than 10.5. At the end of the last addition, the reaction was stopped with acid, followed by washing with distilled water and vacuum filtration. The system 0.016 g TEMPO/0.5 mL NaClO/0.9 g $NaClO_2$ was followed for sulfate pulp immersed in 0.1 M phosphate buffer (pH = 6.8) for 24 h at 60 °C, followed by cooling to room temperature, subsequently washed with distilled water and filtered under vacuum.

Both suspensions passed twice through a GEA Panther NS 3006L homogenizer (GEA, Düsseldorf, Germany). This equipment has a volume of around 4 L and works with a consistency of 1.5%. The operating parameters were the following: two passes, the first at 500 bar and the second at 1000 bar.

The gels were characterized in terms of dry matter content (% solids), rheology and FTIR. To evaluate dry matter content of the nanocellulose gel, the sample (2 mL) was previously weighed (w_i) and subsequently dried in an oven at 105 °C until constant weight. After the sample was cooled in a desiccator, it was weighed again (w_f). The determination of solids content was given in percentage according to the following equation:

$$\%\ Solids = 100 - \frac{w_i - w_f}{w_i}$$

The rheological study of the nanocellulose gels was performed on the HAAKE RS 150 rheometer (Haake, Vreden, Germany), using plate–cone geometry and sensor C35/2°, that is, 35 mm in diameter and 2° angle. Tests were carried out at 23 ± 2 °C and 50 ± 3% relative humidity (RH). The control stress (CS) mode was performed in a measurement range between 0 and 200 Pa.

To investigate the organic compounds of the gels, FTIR analysis was recorded in a Nicolet iS10 smart iTRBasic (Thermo Fisher Scientific, Waltham, MA, USA) in the range of 600–4000 cm^{-1}, with 64 scans and a resolution of 4 cm^{-1}, normalizing the results acquiring previously the background spectra.

2.6. Production and Characterization of Nanocellulose Films

The nanocellulose films were produced using the solvent casting methodology. Initially, the diluted nanocellulose suspensions (1%, w/w) were mixed with glycerol (25%, w/w in relation to nanocellulose) as the plasticizer. This procedure was performed at room temperature for 15 min, maintaining stirring at 300 rpm. For better homogenization, the mixture was taken to the Ultra-Turrax (IKA, Staufen, Germany) for 2 min at 6000 rpm. Subsequently, to eliminate the air created during this process, the blend was placed in a low pressure rotavapor for approximately 30 min. Finally, the mixture was poured into Petri dishes and dried at 60 °C for 6 h in an oven with air circulation. The films were then stored at 50 ± 3% RH and 23 ± 2 °C for further characterization.

For the wax coating, 3 mg of extracted wax was mixed with 4 g of dichloromethane in a test tube placed in a polyethylene glycol (Merck, Darmstadt, Germany) bath at 30 °C for 90 min. Subsequently, molten wax was applied to the surface of nanocellulose films (0.2 g) with a heated glass rod.

To ensure the uniform application of wax onto the film surface, the film was placed on a preheated glass plate. A small volume of wax solution was then poured along one edge of the film, and a preheated glass rod was used to spread the wax while applying light and even pressure.

The single-sided wax-coated films were dried at room temperature and afterward characterized. For this purpose, structural properties, transparency, contact angle, surface energy, water vapor permeability, FTIR and DSC tests were performed.

Regarding the structural properties of the films, specifically grammage, thickness and density were evaluated. Grammage was assessed by the mass-to-area ratio ($g.m^{-2}$) following the ISO 536:1995 standard [13]. Thickness (μm) was measured on a digital micrometer, Adamel Lhomargy (model MI 20) (Saint Baldoph, France), following the ISO 534:2011 standard [14], obtaining five random readings for each film. Following the same standard protocol, the density ($g.cm^{-3}$) of the films was determined by the ratio between grammage and thickness.

Transparency was accessed on the Technidyne Color Touch 2 spectrophotometer, (Technidyne, New Albany, IN, USA) following the ISO 22891 standard [15], using the D65 illuminant and the 10° observer. Two measurements were taken for each type of film.

Contact angle measurements were made by applying the sessile drop method on an OCAH 200, DataPhysics Instruments (DataPhysiscs, Filderstadt, Germany). At least six measurements were performed for each film. Three reference liquids (deionized water, ethylene glycol and diiodomethane) were used to estimate the surface free energy of the films (total, dispersive and polar components) following the Owens, Wendt, Rabel and Kaelble (OWRK) approach [16].

To assess water vapor barrier properties, the desiccant method of ASTM E96-22 standard [17] was followed at 23 ± 2 °C and 50 ± 3% RH. Firstly, WVTR was evaluated and afterward the water vapor permeability (WVP) of the films was determined. For this purpose, using an analytical balance, weight changes (Δw) were recorded over a period of 48 h every 2 h. After that, the graph of mass variation as a function of time allowed the assessment of the slope of the straight line (Δw/Δt). The WVTR was reached through the quotient between this value and the exposed sample area (m^2). Lastly, the WVP was determined using the WVTR values multiplied by the film thickness and dividing by the vapor pressure on each side of the film. Two replicate samples were carried out. This method measured the amount of water vapor that diffused through the film and was absorbed by the desiccant placed beneath it. The water vapor that permeated the film was achieved by the increase in mass of the desiccant.

The DSC technique was used to study the energy involved in the chemical changes of the films when subjected to thermal variations. This analysis was carried out in the Netzsch DSC 204 calorimeter, Selb, Germany, using a temperature range between 30 and 500 °C and heating rate of 5 °C/min in an inert atmosphere. For all analyses, respective baselines were initially obtained, the thermograms being corrected accordingly.

The FTIR technique was used to characterize the CNF films following the same procedure described previously for the nanocellulose gels.

To observe the surface morphology of the nanocellulose films by scanning electron microscopy (SEM), a small sample of each film was fixed with carbon glue onto an aluminum support. Subsequently, they were coated with a layer of gold in a Quorum Q150R ES metal evaporator operating at 45 mA. The observation of the microstructure of the film surfaces was performed in a Hitachi S-3400N microscope (Hitachi, Ibaraki, Japan) at 10 kV acceleration voltage.

3. Results and Discussion

3.1. Chemical Analysis of the Wax

The chemical analysis of the extracted wax is represented by the chromatogram in Figure 1.

Fifteen compounds present in the wax are identified with the compound with the highest incidence being nonacosane. The compounds with relative percentage greater than 1% are nonacosane, 1,21-docosadiene, pentacosane, tetracosanal, eicosane, hexacosanal and triacontane. In addition, other minor compounds such as aldehydes, ketones, alcohols and alkenes are found.

This GC-MS analysis was also carried out on the acidic and neutral parts of the X-7 and X-8 fatty acids, to find out their components. The acidic parts to be analyzed by GC-MS were previously esterified with diazomethane to prepare the corresponding methyl esters and to perform the identification of the fatty acids with the Wiley and NIST databases.

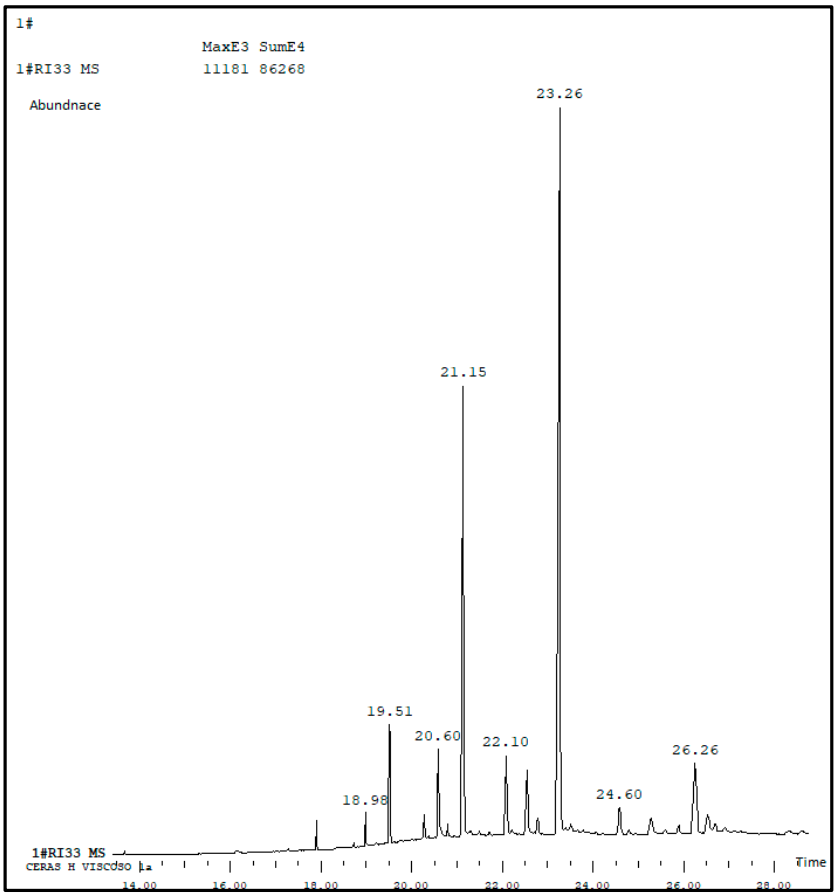

Figure 1. Wax chromatogram.

The results can be seen in Figures 2 and 3, respectively, for X-7 and X-8.

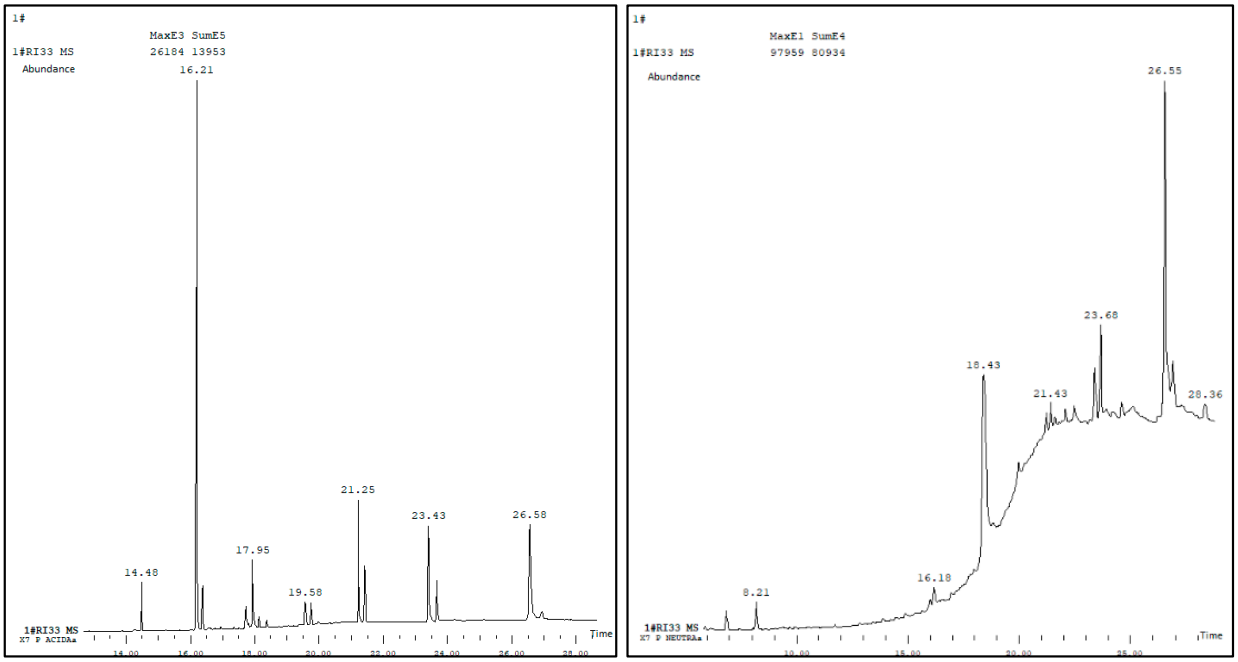

Figure 2. Chromatogram of the fatty acid X-7, P-acidic (**left**) and P-neutral (**right**).

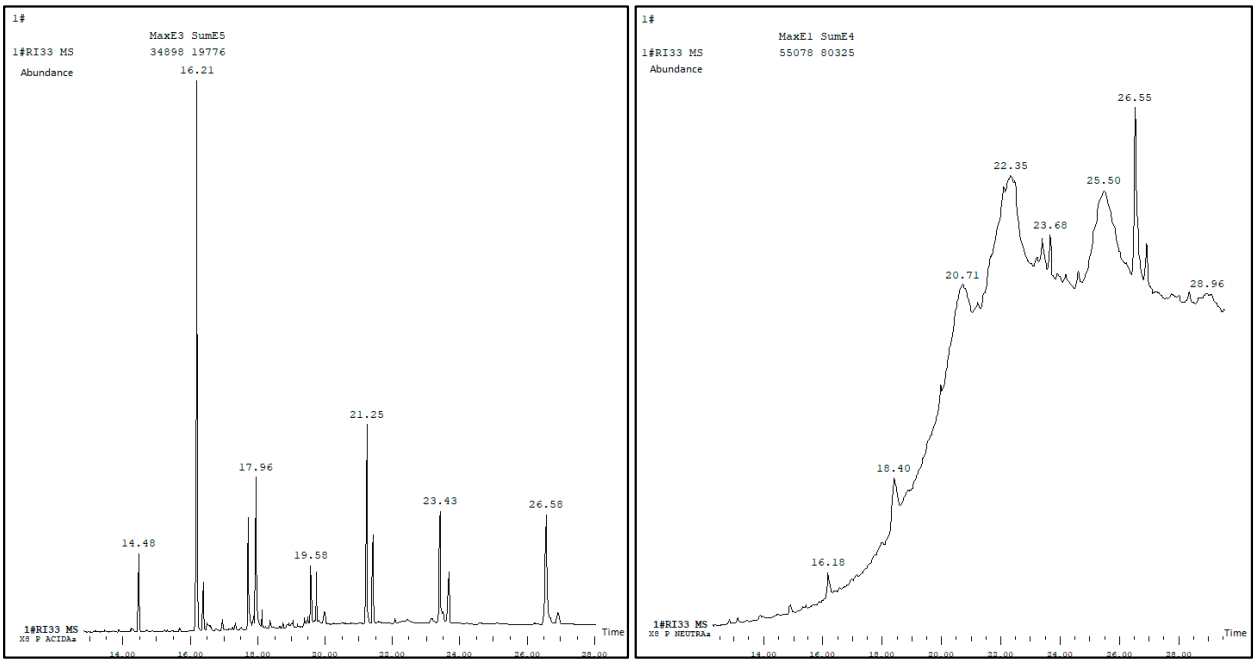

Figure 3. Chromatogram of fatty acid X-8, P-acidic (**left**) and P-neutral (**right**).

It can be observed that the compound with the highest incidence, in the case of the acidic part of the X-7 and X-8 fatty acids, is the methyl 9(Z)-octadecenoate and 9(Z)-octadecenoic acid, with around 31% and 42%, respectively, in relation to the total value. In the case of the neutral part of the fatty acids, the compound with the highest quantity is methyl hexacosanoate; however, large quantities of other methyl esters were also obtained.

Oxo-acids, epoxy-acid and diacids are also identified in the acidic parts. In the neutral parts of the hydrolysis, natural methyl esters of the different acids and some aldehydes are identified.

3.2. Characterization of Nanocellulose Gels and Films

3.2.1. Solids Content of CNF Gels

The results obtained for both gels on solids content are quite similar and slightly higher than 1% in CNF, more precisely 1.039 to CNF_1 and 1.078 to CNF_2, with the main constituent being water. The low CNF content of these gels is associated with their stability and has been reported in the literature by other authors [18].

At 1% concentration, CNF suspensions are more stable due to fibril network formation and its high viscosity. The gel-like properties exhibited by these suspensions prevent the mobility of fibrils and reduce the probability of aggregation and settling. Stability is enhanced because Brownian motion is constrained, and the nanofibers are confined in place.

3.2.2. Rheology of CNF Gel

The results of the rheological analyses of CNF gels are shown in Figure 4**.** Both CNF gels present similar rheological flows. CNF_1 and CNF_2 gels exhibit shear-thinning behavior, as the shear stress increases with the increasing strain rate. As mentioned previously, CNF_1 and CNF_2 gels come from different chemical pulps, respectively, sulfite and sulfate. Differences in the properties of these two pulps have been reported in the literature [19]. Shear-thinning is common in nanocellulose suspensions due to the orientation and releasing of nanofibers under shear. CNF_2 shows a higher shear stress at all strain rates compared with CNF_1, indicating that CNF_2 has a stronger internal network structure, revealing

higher viscosity [20]. CNF_1 exhibits lower shear stress, probably due to its slightly lower solids content. At lower concentrations, the resistance to flow decreases because there are fewer interactions between the particles and the medium. Consequently, more diluted suspensions, with pseudoplastic behavior, generally have lower viscosity and shear stress.

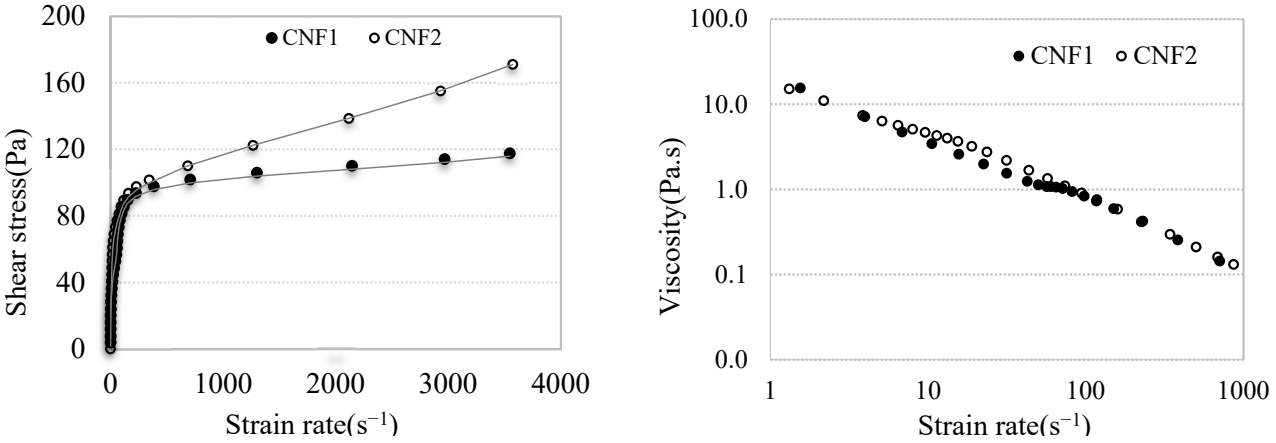

Figure 4. Rheological study.

CNF_1 gel exhibits a lower shear stress, probably due to the slightly lower solids content and weaker fibril interactions. This result can also suggest that films produced from CNF_1 gel may exhibit weaker mechanical properties compared with films produced from CNF_2 gel [21].

Two regions are observed. For the low strain rate, less than 1000 s^{-1}, both gels show a rapid increase in shear stress, characteristic of yield stress behavior [22]. Concerning the high strain rate region, CNF_1 tends to plateau, suggesting that the increase in shear stress becomes less significant. CNF_2 continues to increase more significantly, indicating a greater resistance to flow and therefore higher viscosity. These differences can be explained by the higher nanocellulose concentration of CNF_2 gel, which may provide stronger hydrogen bonding. This result may be confirmed by the FTIR results of the films, where the hydrogen bond band at 3300 cm^{-1} shows a higher intensity for the CNF_2 film compared with the CNF_1 film. Differences in surface chemistry could also influence the rheological behavior. CNF_2 gel has a strong network structure and consequently higher viscosity than CNF_1, requiring more stress to achieve the same strain rate.

In the same figure, the graph on the right reports the viscosity of the CNF gel as a function of the shear rate. The viscosity of both gels decreases sharply with the increasing shear rate. At the beginning, when shear values are low, the viscosity of gels is very high due to the organized network of fibrils. As the shear stress increases, the network structure is slowly broken, and the viscosity progressively decreases due to the alignment of fibrils in the flow. The slightly higher viscosity of the CNF_2 gel could be associated with the fibril size and crystallinity. These results are also reported by other authors [22,23].

3.2.3. FTIR of CNF Gels and CNF Films

The spectra of the CNF gels are presented in Figure 5, where the full overlaps of both spectra stand out.

Three bands can be observed as follows: one quite pronounced at 3300 cm^{-1}, representing hydrogen bonds. This band is related to the stretching vibration of the O–H groups essentially due to the presence of water and hydroxyl groups of cellulose. The hydroxyl group is confirmed by the presence of another band at 1634 cm^{-1}, which signals the results from H–O–H bending of absorbed water. This pick is typical for samples with a large

amount of water [24]. At the fingerprint region, a clear band appears with a pick near 600 cm^{-1}, which may be related to out of plane C–H bending.

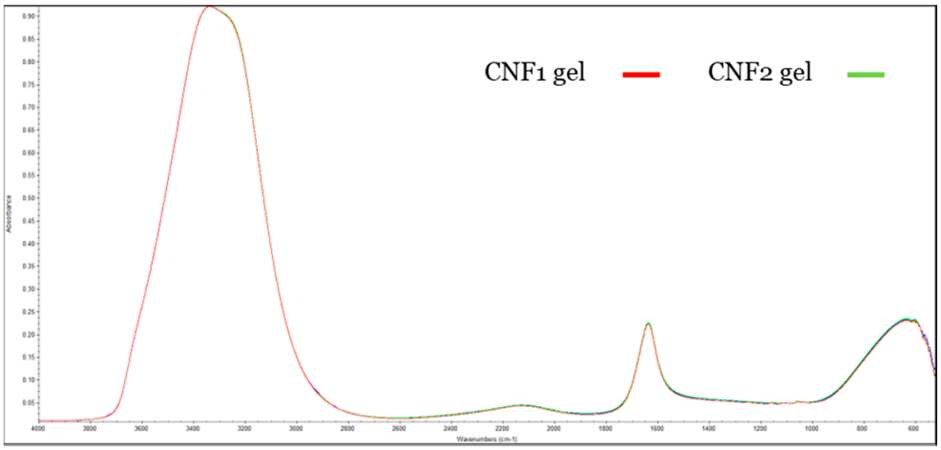

Figure 5. FTIR of CNF gels.

Figure 6 shows the FTIR spectra of the CNF films, uncoated CNF_1 and CNF_2 and the wax-coated, respectively, WC CNF_1 and WC CNF_2. The spectra of the uncoated films show similar peaks, indicating that they assign common functional groups but with different peak intensities, suggesting variations in composition or surface chemistry [19].

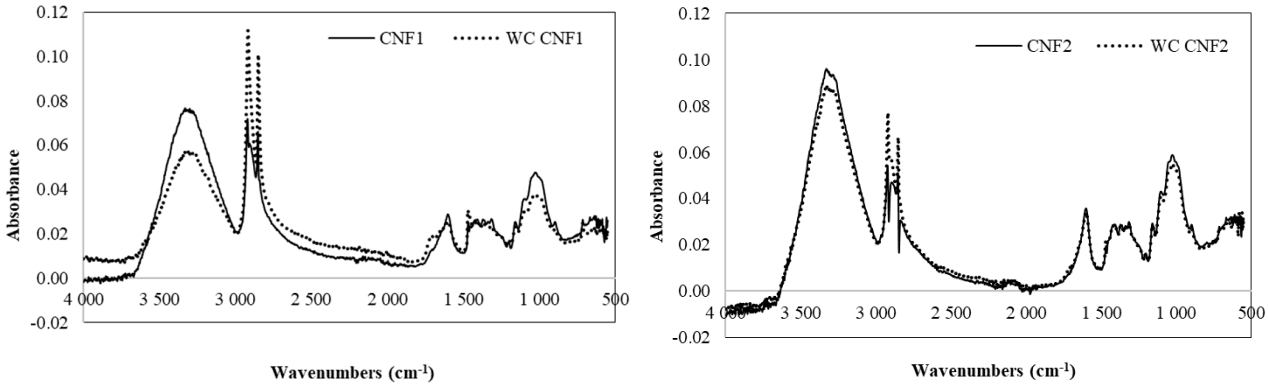

Figure 6. FTIR of uncoated and wax-coated CNF films.

Specific peaks appear between 1200 and 1700 cm^{-1} for CNF_1 and CNF_2 film FTIR spectra, recording the oxidative process TEMPO. One band, near 1600 cm^{-1}, is attributed to the C=O bond in the COONa groups, and another band is assigned to C-O symmetric stretching of dissociated carboxyl groups.

The CNF_2 film shows higher intensity at 3300 cm^{-1} compared with the CNF_1 film. This band is associated with the stretching vibration of the O–H groups of cellulose, followed by the presence of another band at 1634 cm^{-1}, which also has higher intensity. Two peaks arise between 2800 and 3000 cm^{-1} corresponding to C–H bond stretching vibrations of cellulose. The CNF_1 film shows a more intense peak, probably due to the greater number of alkyl groups. This result could indicate more hydrophobicity of these films, which is confirmed by the greater water contact angle compared with CNF_2 films. Between 1720 and 1620 cm^{-1}, two absorption bands appear in the CNF_1 film that are not detected for the CNF_2 film. These bands may be associated with C=O double bonds, since sulfite pulps contain a higher content of carbonyl groups compared with sulfate pulps [19]. Also, at the fingerprint region, between 900 and 1200 cm^{-1}, different intensities for both CNF films are

detected; CNF_2 shows greater intensity for C–O stretching and C–O–C vibrations related to the glycosidic bonds. This result reveals that both CNFs have different surface chemistries.

The spectrum of wax-coated films, displayed in the same figure, also shows a similar profile. However, compared with uncoated films, a reduction in the intensity of absorption at 3300 cm^{-1} and an increase in absorption bands between 2800 and 3000 cm^{-1} is observed. This intensification may result from the stretch, symmetrical or asymmetrical, of the C–H group of alkanes and the CH_2 group of methylene in the lipid chains. This result confirms the effectiveness of the wax coating. Between 2800 and 3000 cm^{-1}, C–H stretching takes place; in this region, the WC CNF films show a more pronounced peak comparative with the uncoated films. This result suggests the presence of additional alkyl (–CH, $–CH_2$, $–CH_3$) functional groups from the wax [25], which is expected since the waxes are composed of long-chain hydrocarbons. In the range of 1620 and 1670 cm^{-1} where the carbonyl group (C=O) responds, the peaks that appear in CNF_1 do not appear on the coated film. The fingerprint region between 1000 and 1500 cm^{-1} shows subtle differences, suggesting additional functional groups associated with wax. The greater intensity of this band for WC CNF_1 indicates the presence of ester or carbonyl groups from the wax components.

3.2.4. DSC of CNF Films

To evaluate the thermal properties of uncoated and wax-coated CNF films, DSC analyses were performed, and graphical results are shown in Figure 7. Between 50 and 120 °C a pronounced endothermic peak is observed, which is attributed to water evaporation absorbed by both samples [26]. The highest intensity of this peak is related to the moisture content of each film. This result agrees with FTIR results, which reveal a greater number of hydrogen bonds in CNF_2.

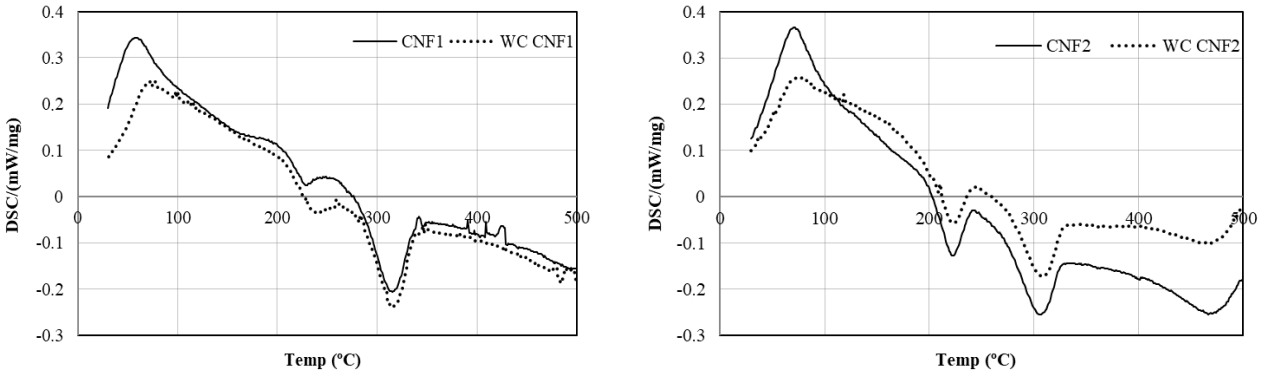

Figure 7. DSC of uncoated and wax-coated CNF films.

Between 210 and 325 °C, both CNF films exhibit two exothermic events related to the degradation of cellulose, suggesting the presence of both TEMPO-oxidized CNF and partially oxidized cellulose. This result is also previously reported [27]. The CNF_1 film decomposes at a slightly higher temperature, suggesting better thermal stability, possibly due to different fiber structures from the sulfite process. The slightly lower decomposition temperature of CNF_2 may be attributed to higher cellulose purity from the sulfate pulping process. Finally, for temperatures above 350 °C, residual decomposition such as decarbonylation to CO and decarboxylation to CO_2 may occur [28]. In this region, smaller peaks can be observed for CNF_1 that did not appear for CNF_2, attesting to the complete decomposition of the latter at lower temperatures. Regarding wax-coated films, the greatest changes are recorded in CNF_1 films. Comparative with uncoated films, the WC CNF_1 film shows a reduced endothermic peak around 80–100 °C. This result suggests that the hydrophobic character of the wax reduces water absorption of CNF films, making them more suitable for applications requiring moisture barrier properties. This outcome can be

validated by the WVTR results of these samples. Between 150 and 280 °C, both curves are relatively stable, but CNF_1 shows a slightly higher baseline heat flow, indicating potential thermal relaxation or rearrangement of cellulose chains against WC CNF_1, which shows a smoother transition, suggesting that the wax coating provides thermal stability in this range. Between 280 and 350 °C, coated and uncoated films exhibit a significant exothermic event attributed to the thermal degradation of cellulose. The WC CNF_1 peak is broader and slightly shifted to higher temperatures, indicating greater thermal stability of this sample due to the wax coating, which slows down decomposition. In post-decomposition regions, more specifically after 350 °C, wax-coated films show a slightly stable baseline, suggesting that wax may act as a barrier, reducing oxidation or final degradation at high temperatures.

3.2.5. Grammage, Thickness, Density and Transparency of CNF Films

CNF films were characterized according to their grammage, thickness, density and transparency, being the results reported in Table 1. Although the same grammage was intended for all the produced films, some differences were observed in their experimental values. The actual grammage of the CNF_1 films is lower than that of the CNF_2 films. This discrepancy may be attributed to differences in the structure of the suspensions. So, if CNF_1 retains more free water, the mass measured in the wet state could be overestimated. However, after drying, the actual dry mass would be lower, resulting in a reduction in grammage.

Table 1. Structural properties of CNF films (results presented as mean ± standard deviation).

Properties	CNF_1	WC CNF_1	CNF_2	WC CNF_2
Grammage ($g.m^{-2}$)	40.18 ± 0.32	40.68 ± 0.21	44.65 ± 0.37	45.12 ± 0.17
Thickness (μm)	38.25 ± 1.39	38.39 ± 0.79	37.98 ± 1.82	38.19 ± 0.68
Apparent density ($g.cm^{-3}$)	1.05	1.06	1.17	1.18
Transparency (%)	79.6 ± 1.51	78.24 ± 0.98	94.1 ± 1.10	91.6 ± 0.90

Higher grammage may imply a denser material; the CNF_2 film has a thicker fibrous matrix and, consequently, higher apparent density, and probably the sulfate pulp fibers compact better than the sulfite pulp fibers due to their morphology [19] and crystallinity [29].

The thickness of the films, coated and uncoated, is approximately the same and close to 38 μm. It is worth noting that the film with the highest grammage (CNF_2) is not the thickest, but rather CNF_1. These results allow us to conclude that the CNF_1 fiber matrix must include a greater amount of air, which can be reinforced by the apparent density values. Regarding transparency, the values vary between 79.6% for CNF_1 films and 94.1% for CNF_2 films. The greater transparency of the CNF_2 film may be a result of the size of the cellulose microfibrils, the degree of homogenization and surface roughness [30]. Fiber morphology and alignment reduce light scattering and increase light transmission. Furthermore, the CNF_2 film has a lower density and, consequently, less air in the fibrous matrix, which can also influence transparency, since air has a lower refractive index compared with cellulose. These results are corroborated by other published works [31].

Regarding the WC CNF films, it can be highlighted that the wax coating does not result in a significant increase in grammage and thickness, as only an increase of less than 1% in apparent density is obtained. However, regarding the transparency of coated films, a slight decrease is recorded compared with uncoated films. The transparency of CNF films decreases by 1.7% and 2.7%, respectively, for CNF_1 and CNF_2 after wax coating.

Natural wax has a higher refractive index [32] compared with nanocelluloses; consequently, it increases light reflection while reducing transmission.

3.2.6. Water Vapor Permeability of Films

Water vapor permeability is a fundamental property that measures a material's ability to allow water vapor molecules to pass through its thickness. This property is especially relevant in applications where moisture barrier is crucial, such as food packaging. The results of this property are shown in Table 2. Regarding the permeability rate, WVTR, the lowest value, stands out for CNF_2 films, corroborating what is expected, since these films have higher density. The compaction of the fibrous matrix makes it difficult for water molecules to pass through, and less water can penetrate through the film, as already mentioned [33].

Table 2. WVTR and WVP for CNF films (results presented as mean ± standard deviation).

Properties	CNF_1	WC CNF_1	CNF_2	WC CNF_2
WVTR ($g.m^{-2}.day^{-1}$)	264.0	49.2	219.2	77.8
WVP ($g.Pa^{-1}.day^{-1}.m^{-1}$)	7.03×10^{-6}	1.39×10^{-6}	6.03×10^{-6}	3.0×10^{-6}

WVTR values obtained in previous studies are comparable to those obtained in this research work for the uncoated CNF films [34,35].

Regarding the results of the wax-coated films, it can be said that wax coating is highly effective as it significantly reduces the WVTR for both films, allowing less water vapor to penetrate through the film. WC CNF_1 and WC CNF_2 show a decrease of 81.4% and 64.5%, respectively. Interestingly, WC CNF_1 has a lower WVTR, indicating that CNF_1 film benefits more from wax coating, mainly because its initial porosity allows better wax penetration and sealing [33]. Comparable results are obtained by [11].

Wax coating of CNF films is an effective strategy to reduce water vapor permeability, addressing one of the main limitations of pure nanocellulose materials. This modification increases the films' suitability for moisture-sensitive applications while maintaining its biodegradable and sustainable advantages.

The observed improved water vapor barrier properties of wax-coated CNF films can be explained by the combination of chemical, physical and structural mechanisms. Chemically, the long-chain hydrocarbons and esters of waxes given a hydrophobic barrier prevent water molecules from reaching the underlying CNF matrix, lowering the WVTR. Physically, the wax fills surface pores, lowering the roughness and eliminating pathways for vapor diffusion (SEM images support this statement).

3.2.7. Contact Angle and Surface Energy of Films

Contact angle and surface free energy are fundamental parameters that play a crucial role in understanding the interactions between liquids and solid surface. The water contact angle refers to the angle formed between the interface of a liquid and the surface of the film and reveals its hydrophilicity. Surface free energy is a fundamental property that describes the tendency of a surface to interact with other materials, representing the amount of energy required to create a unit surface area on a material. Surface free energy influences crucial properties such as wettability, adhesion and interfacial behavior. Understanding and controlling this characteristic is essential in several applications.

The results obtained for water contact angle, total energy, dispersive and polar components are presented in Table 3. The hydrophilic character of CNF-based films is confirmed. However, a considerable improvement in the hydrophobicity of CNF films is achieved after

wax coating, exhibiting a water contact angle higher than 100°. The wax coating significantly increases the water contact angle, which means a drastic increase in hydrophobicity.

Table 3. Water contact angle and surface free energy (results presented as mean ± standard deviation).

Films	CA_{Water}	Surface Energy ($mN.m^{-1}$)		
		Total	Dispersive	Polar
CNF_1	52.53 ± 2.01	46.05	28.85	17.19
CNF_2	49.96 ± 2.45	49.63	29.11	20.52
WC CNF_1	110.93 ± 1.61	28.76	28.75	0.01
WC CNF_2	108.17 ± 1.03	28.93	28.91	0.02

The values obtained for CNF films are corroborated by previous studies [11,36–38], where the contact angle varies between 30° and 50° for CNF films without any additives.

Before coating, the CNF_2 film exhibits a higher polar component in contrast with CNF_1, suggesting a stronger hydrogen bonding capacity and thus a more hydrophilic character. This result can be confirmed by the FTIR spectrum shown in Figure 6, where a high intensity peak can be observed at 3300 cm^{-1}. Furthermore, this result can also be explained by the type of pulp, since sulfate (kraft) pulp tends to preserve or expose more polar functional groups, such as hydroxyls and carboxyl groups on the nanocellulose surface. In contrast, sulfite pulp may result in fewer of these groups due to differences in the chemical treatment, leading to a lower polar component on surface films.

After coating, the CNF films exhibit lower surface energy than the uncoated films. About a 40% decrease in total surface energy is achieved. Since the dispersive component remains almost unchanged in all samples, we can state that the reduction in the total surface energy is determined by polar interactions. A reduction of almost 100% in the polar component is observed. Effectively, the wax coating virtually eliminates the polar component, which is consistent with the presence of a hydrophobic non-polar wax layer. Therefore, WC CNF films are more water repellent and consequently more suitable for applications requiring moisture resistance. These results are in agreement with those reported previously for nanocellulose papers with different lignin contents [39].

3.2.8. Surface Morphology of Films

Figure 8 shows the SEM images of CNF_1 films, uncoated (left) and wax-coated (right). The images show a remarkable difference in the surface morphology of nanocellulose films. The uncoated CNF film shows a micro-structured fibrous texture typical of pure nanocellulose films. The surface of the wax-coated CNF film displays a smoother and continuous layer. The applied wax layer alters the surface roughness and enhances hydrophobic and barrier properties and how they document the contact angle results with water and the permeability to water vapor.

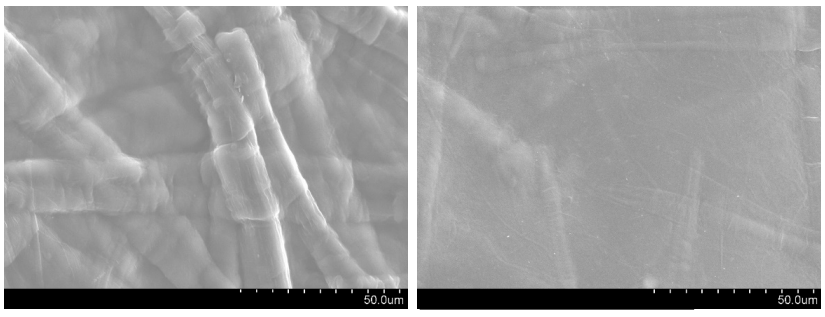

Figure 8. SEM of surface morphology of uncoated CNF films (left) and wax-coated (right) (magnification: 1000×).

4. Conclusions

This study demonstrated that the application of a natural wax coating effectively improved the hydrophobicity of CNF films while maintaining their structural integrity and transparency. The success of wax coating of the films was confirmed through FTIR and the significant increase in water contact angle and a reduction in water vapor permeability, making them more suitable for applications requiring moisture resistance. The water contact angle of wax-coated films increased from 30° to 110°, and a 35% reduction in total energy and 100% in the polar component was achieved. The water vapor permeability results also confirmed the success of the wax application to the surface of the films. The lower value for WC CNF_1 films suggests that these films gained more from the wax coating, likely due to their initial porosity, which allowed better wax penetration and sealing. The obtained results reinforce the feasibility of using bio-based wax to improve the performance of CNF-based films, offering an environmentally friendly alternative to synthetic plastic materials in food packaging. Future research should focus on optimizing the coating process and evaluating the long-term stability of these films under real conditions.

Author Contributions: Conceptualization, A.R. and J.M.R.; methodology, A.R., J.M.R. and Â.L.; validation, A.R.; formal analysis, A.R. and Â.L.; investigation, A.R., J.M.R., R.F. and Â.L.; resources, A.R.; data curation, A.R.; writing—original draft preparation, A.R.; writing—review and editing, J.M.R. and Â.L.; supervision, A.R.; All authors have read and agreed to the published version of the manuscript.

Funding: The authors are very grateful for the support granted by the Research Unit of Fiber Materials and Environmental Technologies (FibEnTech-UBI), through the Project reference UIDB/00195/2020, funded by the Fundação para a Ciência e a Tecnologia, IP/MCTES (FCT) through national funds (PIDDAC), and DOI: 10.54499/UIDB/00195/2020 (https://doi.org/10.54499/UIDB/00195/2020). This work was also supported by resources from the CICS-UBI basic funding with DOI 10.54499/UIDB/00709/2020 (https://doi.org/10.54499/UIDB/00709/2020) and programmatic funding from CICS-UBI with DOI 10.54499/UIDP/00709/2020 (https://doi.org/10.54499/UIDP/00709/2020) with national funds registered in the budget of the FCT.

Institutional Review Board Statement: Not applicable.

Informed Consent Statement: Not applicable.

Data Availability Statement: Data will be availability by request to the corresponding authors.

Conflicts of Interest: The authors declare no conflicts of interest.

References

1. Turbak, A.F.; Snyder, F.W.; Sandberg, K.R. Microfibrillated cellulose, a new cellulose product: Properties, uses and commercial potential. *J. Appl. Polym. Sci. Appl. Polym. Symp.* **1983**, *37*, 815–827.
2. Kim, J.H.; Shim, B.S.; Kim, H.S.; Lee, Y.J.; Min, S.K.; Jang, D.; Abas, Z.; Kim, J. Review of nanocellulose for sustainable future materials. *Int. J. Precis. Eng. Manuf. Green. Technol.* **2015**, *2*, 197–213. [CrossRef]
3. Mokhena, T.C.; John, M.J. Cellulose nanomaterials: New generation materials for solving global issues. *Cellulose* **2020**, *27*, 1149–1194. [CrossRef]
4. Nogi, M.; Iwamoto, S.; Nakagaito, A.N.; Yano, H. Optically Transparent Nanofiber Paper. *Adv. Mater.* **2009**, *21*, 1595–1598. [CrossRef]
5. Siró, I.; Plackett, D. Microfibrillated cellulose and new nanocomposite materials: A review. *Cellulose* **2010**, *17*, 459–494. [CrossRef]
6. Stark, N.M. Opportunities for cellulose nanomaterials in packaging films: A review and future trends. *J. Renew. Mater.* **2016**, *4*, 313–326. [CrossRef]
7. Hubbe, M.A.; Ferrer, A.; Tyagi, P.; Yin, Y.; Salas, C.; Pal, L.; Rojas, O.J. Nanocellulose in thin films, coatings, and plies for packaging applications: A review. *BioResources* **2017**, *12*, 2143–2233. [CrossRef]
8. Song, J.; Rojas, O.J. Approaching super-hydrophobicity from cellulosic materials: A review. *Nord. Pulp Pap. Res. J.* **2013**, *28*, 216–238. [CrossRef]

9. Costa, V.L.D.; Simões, R.M.S. Hydrophobicity improvement of cellulose nanofibrils films by stearic acid and modified precipitated calcium carbonate coating. *J. Mater. Sci.* **2022**, *57*, 11443–11459. [CrossRef]
10. Forsman, N.; Lozhechnikova, A.; Khakalo, A.; Johansson, L.S.; Vartiainen, J.; Österberg, M. Layer-by-layer assembled hydrophobic coatings for cellulose nanofibril films and textiles, made of polylysine and natural wax particles. *Carbohydr. Polym.* **2017**, *173*, 392–402. [CrossRef]
11. Österberg, M.; Vartiainen, J.; Lucenius, J.; Hippi, U.; Seppälä, J.; Serimaa, R.; Laine, J. A fast method to produce strong NFC films as a platform for barrier and functional materials. *ACS Appl. Mater. Interfaces* **2013**, *5*, 4640–4647. [CrossRef] [PubMed]
12. Doan, C.D.; To, C.M.; Vrieze, M.D.; Lynen, F.; Danthine, S.; Brown, A.; Dewetthink, K.; Patel, A.R. Chemical profiling of the major components in natural waxes to elucidate their role in liquid oil structuring. *Food Chem.* **2017**, *214*, 717–725. [CrossRef] [PubMed]
13. *ISO 536:1995*; Paper and Board—Determination of Grammage. International Organization for Standardization: Geneva, Switzerland, 1995.
14. *ISO 534:2011*; Paper and Board—Determination of Thickness, Density and Specific Volume. International Organization for Standardization: Geneva, Switzerland, 2011.
15. *ISO 22891:2013*; Paper—Determination of Transparency by Diffuse Reflectance Method. International Organization for Standardization: Geneva, Switzerland, 2013.
16. Çıtak, A.; Yarbaş, T. Using contact angle measurement technique for determination of the surface free energy of B-SBA-15-x materials. *Int. J. Adhes. Adhes.* **2022**, *112*, 103024. [CrossRef]
17. *ASTM E96-22*; Standard Test Methods for Water Vapor Transmission of Materials. ASTM International: West Conshohocken, PA, USA, 2022.
18. Sharma, A.; Mandal, T.; Goswami, S. Dispersibility and Stability Studies of Cellulose Nanofibers: Implications for Nanocomposite Preparation. *J Polym Env.* **2021**, *29*, 1516–1525. [CrossRef]
19. Iglesias, M.C.; Gomez-Maldonado, D.; Via, B.K.; Jiang, Z.; Peresin, M.S. Pulping processes and their effects on cellulose fibers and nanofibrillated cellulose properties: A review. *Prod. J.* **2020**, *70*, 10–21. [CrossRef]
20. Kulichikhin, V.G.; Malkin, A.Y. The Role of Structure in Polymer Rheology: Review. *Polymers* **2022**, *14*, 1262. [CrossRef]
21. Barbash, V.A.; Yakymenko, O.S.; Yashchenko, O.V.; Zakharko, R.M.; Myshak, V. D Preparation of hemp nanocellulose and its use to improve the properties of paper for food packaging. *Cellulose* **2022**, *29*, 8305–8317. [CrossRef]
22. Moberg, T.; Sahlin, K.; Yao, K.; Geng, S.; Westman, G.; Zhou, Q.; Oksman, K.; Rigdahl, M. Rheological properties of nanocellulose suspensions: Effects of fibril/particle dimensions and surface characteristics. *Cellulose* **2017**, *24*, 2499–2510. [CrossRef]
23. Honorato, C.; Kumar, V.; Liu, J.; Koivula, H.; Xu, C.; Toivakka, M. Transparent nanocellulose-pigment composite films. *J. Mater. Sci.* **2015**, *50*, 7343–7352. [CrossRef]
24. El-Sakhawy, M.; Kamel, S.; Salama, A.; Tohamy, H.A.S. Preparation and infrared study of cellulose based amphiphilic materials. *Cellul. Chem. Technol.* **2018**, *52*, 193–200.
25. Zhu, M.; Ying, D.; Zhang, H.; Xu, X.; Chang, C. Self-healable hydrophobic films fabricated by incorporating natural wax into cellulose matrix. *Chem. Eng. J.* **2022**, *446*, 136791. [CrossRef]
26. Kian, L.K.; Jawaid, M. Thermal properties of nanocrystalline cellulose and cellulose nanowhisker. *Int. J. Innov. Technol. Explor. Eng.* **2019**, *9*, 5430–5434. [CrossRef]
27. Miao, X.; Lin, J.; Tian, F.; Li, X.; Bian, F.; Wang, J. Cellulose nanofibrils extracted from the byproduct of cotton plant. *Carbohydr. Polym.* **2016**, *136*, 841–850. [CrossRef] [PubMed]
28. Jiang, F.; Hsieh, Y.L. Chemically and mechanically isolated nanocellulose and their self-assembled structures. *Carbohydr. Polym.* **2013**, *95*, 32–40. [CrossRef] [PubMed]
29. Hult, E.L.; Iversen, T.; Sugiyama, J. Characterization of the supermolecular structure of cellulose in wood pulp fibres. *Cellulose* **2003**, *10*, 103–110. [CrossRef]
30. Kim, H.J.; Roy, S.; Rhim, J.W. Effects of various types of cellulose nanofibers on the physical properties of the CNF-based films. *J. Env. Chem. Eng.* **2021**, *9*, 106043. [CrossRef]
31. Boufi, S.; Kaddami, H.; Dufresne, A. Mechanical performance and transparency of nanocellulose reinforced polymer nanocomposites. *Macromol. Mater. Eng.* **2014**, *299*, 560–568. [CrossRef]
32. Tian, L.; Xu, X. Optical Properties and Crystallization of Natural Waxes at Several Annealing Temperatures: A Terahertz Time-Domain Spectroscopy Study. *J. Infrared Millim. Terahertz Waves* **2018**, *39*, 302–312. [CrossRef]
33. Ferrer, A.; Pal, L.; Hubbe, M. Nanocellulose in packaging: Advances in barrier layer technologies. *Ind. Crops Prod.* **2017**, *95*, 574–582. [CrossRef]
34. Nair, S.S.; Zhu, J.; Deng, Y.; Ragauskas, A.J. High performance green barriers based on nanocellulose. *Sustain. Chem. Process* **2014**, *2*, 23. [CrossRef]
35. Herrera, M.A.; Mathew, A.P.; Oksman, K. Barrier and mechanical properties of plasticized and cross-linked nanocellulose coatings for paper packaging applications. *Cellulose* **2017**, *24*, 3969–3980. [CrossRef]

36. Surya, I.; Hazwan, C.M.; Abdul Khalil, H.P.S.; Yahya, E.B.; Suriani, A.B.; Danish, M.; Mohamed, A. Hydrophobicity and Biodegradability of Silane-Treated Nanocellulose in Biopolymer for High-Grade Packaging Applications. *Polymers* **2022**, *14*, 4147. [CrossRef] [PubMed]
37. Lavrič, G.; Oberlintner, A.; Filipova, I.; Novak, U.; Likozar, B.; Vrabič-Brodnjak, U. Functional Nanocellulose, Alginate and Chitosan Nanocomposites Designed as Active Film Packaging Materials. *Polymers* **2021**, *13*, 2523. [CrossRef] [PubMed]
38. Cherpinski, A.; Torres-Giner, S.; Vartiainen, J.; Peresin, M.S.; Lahtinen, P.; Lagaron, J.M. Improving the water resistance of nanocellulose-based films with polyhydroxyalkanoates processed by the electrospinning coating technique. *Cellulose* **2018**, *25*, 1291–1307. [CrossRef]
39. Rojo, E.; Peresin, M.S.; Sampson, W.W.; Hoeger, I.C.; Vartiainen, J.; Lainea, J.; Rojas, O.J. Comprehensive elucidation of the effect of residual lignin on the physical, barrier, mechanical and surface properties of nanocellulose films. *Green. Chem.* **2015**, *17*, 1853–1866. [CrossRef]